Journal of Nuclear Materials 404 (2010) 60–67

Contents lists available at ScienceDirect

Journal of Nuclear Materials

journal homepage: www.elsevier.com/locate/jnucmat

Dynamic analysis and evolution of mixed materials bombarded with multiple ions beams

T. Sizyuk *, A. Hassanein

School of Nuclear Engineering, Purdue University, West Lafayette, IN 47907, USA

ARTICLE INFO

Article history:
Received 23 April 2010
Accepted 20 June 2010

ABSTRACT

Materials modification and response to the impact of energetic particles is an important ongoing research area in several applications. This includes both experimental and theoretical work. We updated and improved our models for the simulation of Ion Transport in Materials and Compounds (ITMC-DYN), part of HEIGHTS package, to now include dynamic changing of materials composition as result of multiple ion beams bombardment and target atoms mixing, segregation, and diffusion. Implemented models consider detail processes of simultaneous and multiple ions penetration and mixing, scattering, reflection, physical and chemical sputtering of composite material atoms, dynamic surface evolution/modification, thermal diffusion, and surface segregation and recombination of species in multicomponent alloys. For benchmarking of the models we compared our simulations results with several recent experimental data for nanoapplications and for the developments of future fusion energy systems. Simulation of tungsten surface evolution and modification under the impact of hydrogen ions with carbon impurities demonstrated good agreement with recent experiments. Details of surface erosion and conditions for blisters formation as a function of fluence and material temperature were also analyzed and explained.

1. Introduction

The area of studying ion beams/target mixing and interactions has many interests and applications such as material surface modification, nanolayers and nanoclusters formation by low energy ions, material erosion lifetime, and plasma contamination in magnetic, inertial fusion, and extreme ultraviolet lithography devices. The scale and the degree of complexity of the processes considered in modeling of such systems vary depending on the application. Ion–target interactions (both electronic and nuclear) and following ions and target atoms motion are usually included in most models in a simple way for studying the dependence of target material erosion on ion beam energy, intensity, and angle of incidence. More accurate analysis of plasma facing materials under plasma particle beams in fusion devices should be able to handle multiple and simultaneous ion beams incidents on target materials operating at high temperatures (around 1000 K and higher). This requires implementation and the interplay of particle diffusion, thermal and chemical erosion of surface, segregation, and molecular surface recombination (hydrogen isotopes) and desorption.

Computer modeling of integrated processes in such systems allows better understanding of the interplay phenomena of ions deposition, target atoms mixing and diffusion, segregation, target surface erosion, and possible compounds formation. The most widely used binary collision approximation (BCA) computer code for studying of ions transport in target, TRIM, is based on ZBL potential for ions/atoms interactions and considers static targets [1,2]. Another version of this code, TRIDYN, is based on KrC potential and has implemented dynamic changing of target composition [3]. We included in our model implementation of three different inter-atomic potentials – ZBL, KrC, and Moliere to study the influence of various potentials on surface modification processes. The dynamic updating of target layers composition in our Ion Transport in Materials and Compounds (ITMC-DYN) code is time-dependent on fluence and on self-consistent contribution of physical processes to accurately simulate actual experimental conditions. For detail analysis of target modification, our models consider all atoms generated cascades including implanted, diffused, and segregated atoms. We implemented graphical user interface with built-in the periodic table of elements and their properties that the user can change in accordance with system simulation of the specific experimental setup.

2. Brief description of ITMC-DYN models

The simulation of Ion Transport in Materials and Compounds [4,5] has been upgraded to now includes the following capabilities: (1) implementation of ZBL, KrC, or Moliere screening functions for the Coulomb potentials in modeling elastic atomic collisions; (2) implementation of combination of LSS and Bethe models and

* Corresponding author. Tel.: +1 765 494 4262; fax: +1 765 496 2233.
E-mail addresses: tsizyuk@purdue.edu (T. Sizyuk), hassanein@purdue.edu (A. Hassanein).

0022-3115/$ - see front matter © 2010 Elsevier B.V. All rights reserved.
doi:10.1016/j.jnucmat.2010.06.031

Ziegler fitting coefficients for the inelastic electronic energy loss; (3) dynamic time-dependent update of target composition; (4) unlimited number of target layers with unlimited number of composite materials; (5) unlimited number of incident ion beams with different parameters; (6) implanted atoms diffusion and mixing; (7) molecular surface recombination and desorption; (8) chemical erosion and surface segregation; (9) graphical interface with built-in periodical table of elements and their properties. ITMC-DYN code is based on Monte Carlo methods for the binary collision approximation and the selection of the struck atom from a compound and for modeling of the atomic collision processes. The code is part of High Energy Interaction with General Heterogeneous Target Systems (HEIGHTS) simulation package developed to study self-consistently target surface evolution processes due to intense particle and energy fluxes impinging on target materials to study erosion lifetime and materials performance in various applications including plasma facing and first wall components of magnetic and inertial fusion devices, targets response in high power accelerators, laser and discharge produced plasma devices for advanced lithography systems, and directed energy lethality for defence applications [6]. A brief description of the models used and implemented in the ITMC-DYN code is given below.

2.1. Ion–atom interaction and inelastic energy loss

The ion–atom and atom–atom elastic interactions are modeled based on the common form of a screened Coulomb potential between the interacting species. The detail procedure of calculating the scattering angle in the center-of-mass system and interaction cross-sections are described elsewhere [4]. Three screening functions were implemented in ITMC-DYN code – (1) Moliere with Firsov screening length; (2) KrC with Firsov screening length; (3) ZBL with universal screening length.

For the inelastic interactions, the code includes two methods for calculating the electronic energy losses – a combination of the Lindhard–Scharff–Schiott (LSS) and Bethe models or using Ziegler fitting coefficients. The LSS-stopping formula is used for ion energies $\leqslant$25 keV/amu [7]. The Bethe stopping power is used for incident ion velocities $v > v_0 Z_1^{2/3}$ [8], where v_0 is Bohr velocity [9]. An interpolation formula proposed by Varelas and Biersack [8] is implemented for calculating the electronic energy loss in the intermediate ions energy range. The detailed description of simulating the inelastic interactions is given in [4].

2.2. Dynamic updating of target materials composition

The target material can compose of many different target layers with any thicknesses. Each layer can be composed of various atoms. The ITMC-DYN code updates the composition of target layers at each time step specified by the user. Motion of ions and atoms in target is modeled using pseudoparticles. One pseudoparticle corresponds to an interval of the particles flux. The weight of the pseudoparticle is calculated as:

$$W = \text{Flux}/\text{Pseudoparticle number}$$

In the simulation with dynamic target atoms update, the actual irradiation/experimental time is also divided into intervals (Δt). At each time interval, Δt, the total contribution of pseudoparticles to the change in each layer composition depends on the number of removed and deposited particles and can be given by:

$$N_i(t + \Delta t) = N_i(t) + W n_i \Delta t / \Delta z \quad (1)$$

where N_i is the atomic density of type i; n_i is the total accumulated number of pseudoparticles of type i; and Δz is the layer thickness.

After recalculation of the total atomic number density N_i in the layer i, a relaxation of the target thickness is performed. The ITMC-DYN has then two options for the control of the atomic density:

1. the number density in the layer is always equal to its initial value; or
2. the number density in the layer depends on the changed layer composition and is equal to the actual number density of the given composition.

Exceeding or decreasing of the above values are regulated by then changing of the layer thickness Δz. The layer thickness Δz is also controlled by the initial layer thickness value Δz_0:

(a) If $\Delta z > 1.5\Delta z_0$, the current layer is divided on two separate layers.
(b) If $\Delta z < 0.5\Delta z_0$, the current layer is added to the layer underneath.

2.3. Particles diffusion in target materials

The implanted atoms during irradiation can move due to the established concentration gradients and thermal diffusion. The time-dependent concentration of the implanted atoms depends on the diffusion of particles in target and is described by Fick's second law:

$$\frac{\partial C(z,t)}{\partial t} = D\frac{\partial^2 C(z,t)}{\partial^2 z} \quad (2)$$

where C is the concentration of the diffusing particles; D is the diffusion coefficient, which depends on the target temperature T and is usually written in the Arrhenius form as:

$$D = D_0 \exp(-E_d/kT) \quad (3)$$

where D_0 is a frequency factor depends on lattice structure; E_d is the diffusion activation energy; and k is Boltzmann's constant.

The inclusion of the diffusion processes is very important in simulating fusion reactor conditions where target materials operate at high temperatures and the diffusion of the incident particles can significantly influence the material surface composition and hence plasma–material interactions and the overall performance of the fusion reactor. The ITMC-DYN calculates the diffusion coefficient of multicomponent materials depending on the target composition as the interpolation of logarithmic values of diffusivity of each component. In our analysis below, we considered in detail the special case for the diffusion of carbon in tungsten because of the wide range of published experimental data for the diffusion of C in W that varies in several orders and most recent values [10] showed dependence of the diffusion coefficient on carbon concentration.

2.4. Surface recombination of hydrogen isotopes in target materials

In special cases the release of the implanted gases such as helium and hydrogen isotopes from target surfaces should be considered in addition to the diffusion processes. Hydrogen isotopes retention and inventory in plasma facing components are very important to understand from both safety and plasma performance points of view. In modeling and simulation of fusion reactor environments the following boundary condition at the surface ($z = 0$) is used to predict the recombination of diatomic molecules (for D_2 and T_2):

$$J(z) = D\frac{\partial}{\partial z}C(z) = K_r C^2(z) \quad (4)$$

where z is distance from the surface normal; K_r is the molecular recombination constant, which can be calculated in various ways as described previously [11–13], for example [13]:

$$K_r(T) = \frac{4\alpha c_1 \exp[(2E_s - E_x)/kT]}{\sqrt{MT}(\rho S_0)^2} \quad (5)$$

where ρ is the target density; α is the sticking coefficient; c_1 is the kinetic theory constant; M is the hydrogen isotope atomic mass; S_0 is the pre-exponential constant for solubility; E_s is the heat of solution; and the surface barrier E_x is given by Hassanein [14]:

$$E_x = \max(E_s + E_d, 0) \quad (6)$$

The solubility, S, is the concentration of hydrogen isotope atoms in the target material that is in equilibrium with the isotope gas at a pressure P given by [14]:

$$S(T,P) = S_0\sqrt{P}\exp(-E_s/kT) \quad (7)$$

In the case of Arrhenius form for the calculation of the recombination rate coefficient, two parameters, the activation energy and a fitting pre-exponential constant, are usually calculated for different temperatures by approximating the experimental values in the permeation studies and by modeling various experimental results [15]. The influence of various forms on the resulting value of the recombination rate was previously studied in detail [14].

2.5. Chemical erosion of carbon-based materials

The chemical erosion of carbon-based materials by hydrogen ions bombardment and interaction has strong dependence on target temperature, ions energy, and flux intensity [16]. The following model for chemical erosion of carbon takes into account all above dependencies for the calculation of carbon chemical sputtering yield [17]:

$$Y_{\text{chem}}(\Gamma, T, E_0) = \frac{6\cdot 10^{19} e^{-\frac{1}{kT}}}{10^{15} + 3\cdot 10^{27} e^{-\frac{2}{kT}}}\left[3 + 200 Y_{\text{phys}}(E_0)\right]\left(\frac{\Gamma_i}{10^{20}}\right)^{-0.1} \quad (8)$$

where Γ is the flux of incident ions in $10^{20}\ \text{m}^{-2}\ \text{s}^{-1}$; E_0 is the initial energy of ions; $Y_{\text{phys}}(E_0)$ is the physical sputtering yield.

The combination of the above model for chemical sputtering yield with calculated value of physical sputtering in dependence on ions energy provides a very good agreement with recent results of the chemical erosion yield determined from spectroscopic measurements in different fusion devices and plasma simulators [16]. The concentration of carbon in mixed target materials and its surface segregation requires additional correction in the evaluation of chemical erosion, therefore the total carbon losses are calculated in our model in correspondence with its concentration in each layer near the surface.

2.6. Surface segregation

The kinetics of surface segregation of various species in multicomponent alloys has many treatments. One of the most known interpretations of this phenomenon is given by du Plessis and van Wyk [18] based on Darken explanation of "uphill" diffusion. According to their theoretical description surface segregation is a diffusional process against the concentration gradient and it is a result of the difference in the chemical potential of the diffusing species from surface to bulk.

The chemical potential of the species in an ideal binary alloy can be written as:

$$\mu = \mu^0 + kT\ln C \quad (9)$$

where μ^0 is the standard chemical potential. The change in the chemical potential of species is related to the change in Gibbs free energy of this system as:

$$\Delta G = \mu_1^{0B} - \mu_1^{0S} + \mu_2^{0S} - \mu_2^{0B} \quad (10)$$

where at the right part of the equation are standard chemical potentials of species 1 and 2 in the bulk and on the surface. And surface segregation in binary alloys in terms of the difference in Gibbs free energy between surface and bulk is given then by du Plessis and van Wyk [18]:

$$\frac{\partial C_s(t)}{\partial t} = \frac{M}{a_1^2} C_1(t)\left[\Delta G + kT\ln\frac{C_1(t)(1-C_s(t))}{C_s(t)(1-C_1(t))}\right]$$
$$\frac{\partial C_i(t)}{\partial t} = MkT\left[\frac{C_{i+1}(t)}{a_{i+1}^2}\ln\frac{C_{i+1}(t)(1-C_i(t))}{C_i(t)(1-C_{i+1}(t))} - \frac{C_i(t)}{a_i^2}\ln\frac{C_i(t)(1-C_{i-1}(t))}{C_{i-1}(t)(1-C_i(t))}\right] \quad (11)$$

where $C_s(=C_0)$ and C_i are the relative concentrations at the top surface and at the ith layer of the bulk respectively; a_i is the thickness of ith layer; ΔG is the segregation energy; and M is the mobility of the species.

The mobility parameter was introduced in the theoretical analysis of surface segregation phenomena in terms of the chemical potential gradient. It was found that the mobility can be related to the diffusion coefficient as [18]:

$$D = MkT\left(1 + \frac{\partial \ln f}{\partial \ln C}\right) \quad (12)$$

where f is the activity coefficient of species and depends on the solution of components in alloys. It was shown in the experiments that the value of the segregation energy depends on the sample temperature [19] and grows with the increase in concentration of the solute species [20].

3. Simulation results

3.1. Influence of the inter-atomic potential and binding energy

The ITMC-DYN has implemented three interaction potentials for modeling ion–atom collisions. The choice of the inter-atomic potential is found to be very important in some cases for understanding material erosion and growth. We studied the influence of the inter-atomic potentials on surface recession or buildup for the case of incident Sb ions with different fluences on Si target. First, we compared the sputtering yields of Sb target bombarded by Sb ions with various energies. Results of the simulation using the different potentials of ZBL, KrC, and Moliere models are presented in Fig. 1. Since the values of the screening function for KrC potential are located between the values of ZBL and Moliere

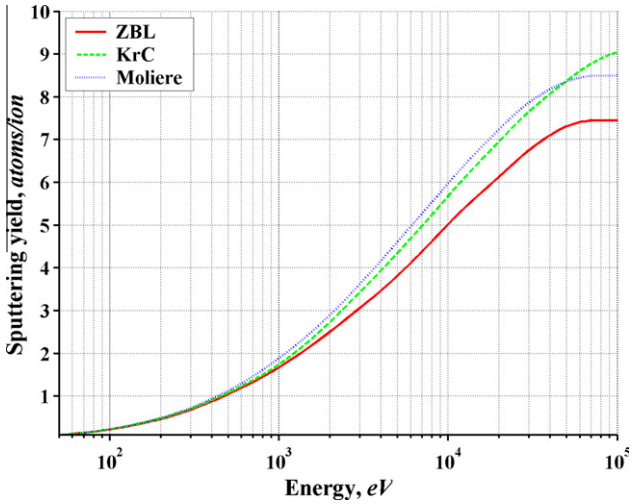

Fig. 1. Self-sputtering of Sb as function of ion energy for different potentials.

potentials with Moliere potential giving the highest value [21], sputtering yields also exhibit similar behavior for a wide range of energy values with deviation at low and high energies. This can be explained by the change in the tendency of the screening functions with increasing function argument and the specific fitting constants for each potential in the calculation procedure of the scattering angle.

These results were obtained with antimony bulk binding energy of 2 eV. The binding energy is defined as the energy needed to take out an interior atom from a normal lattice site position and place it on the surface of the material [22]. In BCA model this value is subtracted from the energy transferred by ions to the struck atom. Some BCA models do not take into account the effect of the bulk binding energy. The value of the binding energy can significantly influence the sputtering yield results especially in the case of low energy ions since it will influence the energy of the struck atom and the number of the subsequent collisions with other target atoms. In the energy range where the sputtering yield is around unity, taking into account the binding energy in numerical simulation can further change the tendency of the surface modification – from erosion to buildup (Figs. 2 and 3)! When the fluence of Sb ions with an incident energy of 300 eV bombarding Si target exceeds a certain value (1–50 $\times$ 10^{20} m^{-2}, depending on the binding energy) the target surface is grown as a result of Sb deposition on the surface. This is because the sputtering yield of Si is small (3×10^{-2}) and the implanted range of Sb is short (about 3 nm) for such ions energy. With increasing irradiation time, the Sb layer covers Si substrate and the subsequent implantation process depends on the interaction of the incident Sb ions with the antimony deposited on the surface. The self-sputtering of Sb without taking into account the binding energy is around 1.23 for ZBL, 1.18 for KrC, and 1.16 for Moliere potentials while this parameter has values of 0.67 for ZBL, 0.7 for KrC, and 0.71 for Moliere potentials when using a Sb binding energy of 2 eV. This causes erosion (Fig. 2) or buildup (Fig. 3) of the surface respectively. In the first case, with increasing the fluence the process of surface modification reaches the steady-state condition with respect to target composition with the formation of antimony layer of ~5 nm thickness.

3.2. Modeling of nanolayers formation

The dynamic part of the ITMC-DYN code was further benchmarked against recent experimental data from the deposition of low energy ions of C and Fe on Si substrate [23]. In these experiments, carbon ions with energy of 50 eV and iron ions with energy of 90 eV were deposited using dose rates varied from 5×10^{19} to 2×10^{20} ions/m^2. During deposition, the Fe and C ionized cathodic arcs were alternately switched on and off, corresponding with the Fe and C layer deposition period respectively. We modeled these experiments using surface binding energies of 7.41 eV and 4.34 eV for C and Fe respectively. Figs. 4 and 5 show the sequence of nanolayers formation and their thicknesses for fluences of 5×10^{19}, 8×10^{19}, 1×10^{20}, and 2×10^{20} ions/m^2. Dual beams of Fe and C ions were simulated alternatively impinging on the Si substrate. This process is repeated to match the experimental conditions of both beams and the total fluence. Figures also show the difference in the models used for the atomic number density. In the first case (Fig. 4) we assumed that the density of the compound of Fe, C, and Si in the area located above the initial surface of Si substrate corresponds to the density of the resulting composition of these atoms. In the second case (Fig. 5), the atomic density was kept equal to its initial value, i.e., the Si atomic density. For comparison with the experimental data, Fig. 6 shows the TEM micrograph of Fe/C multilayers with four bilayer periods: 0.75 nm, 1.25 nm, 2.5 nm, and 5.0 nm [23]. In this experiment, each dual-fluences were repeated five

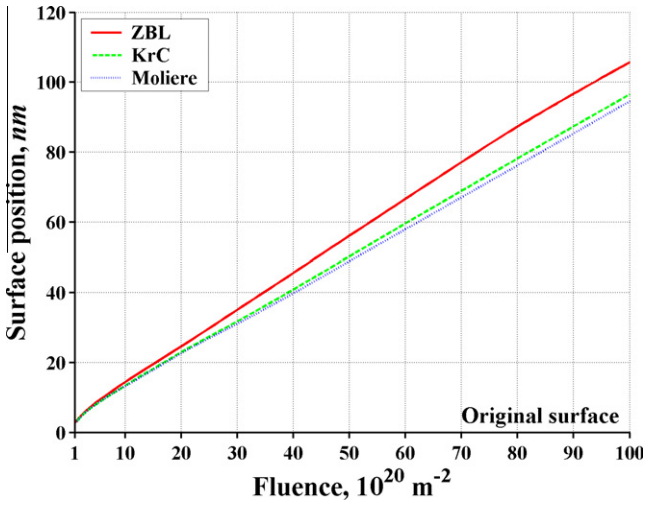

Fig. 3. The case of 2 eV binding energy of Sb in simulation of 300 eV antimony ions implantation in Si substrate.

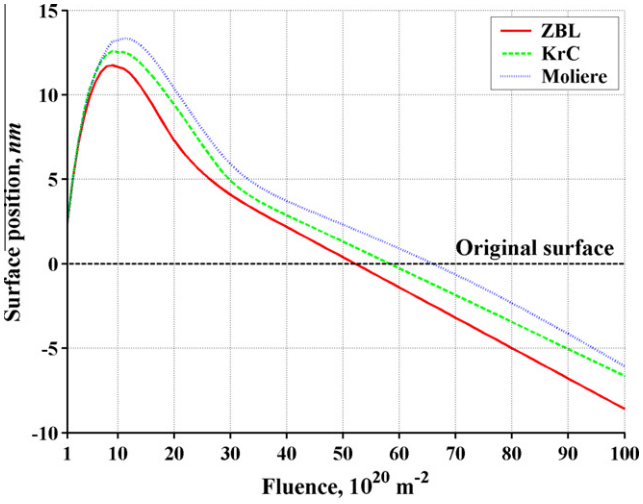

Fig. 2. The case of 0 eV binding energy of Sb in simulation of 300 eV antimony ions implantation in Si substrate.

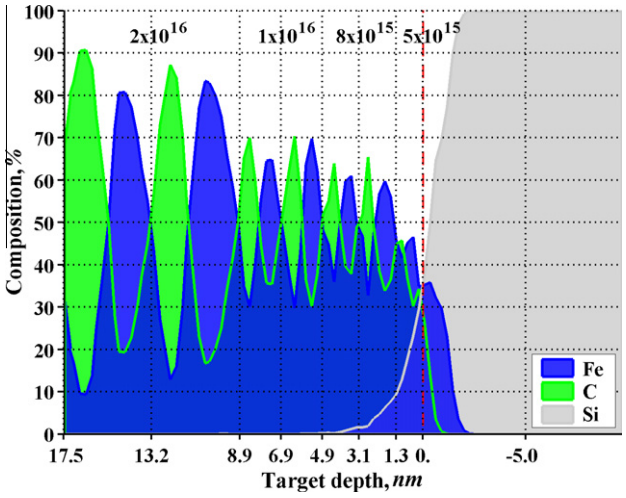

Fig. 4. Four bilayer periods with two bilayers each for fluences of 2×10^{20}, 1×10^{20}, 8×10^{19}, and 5×10^{19} ions/m^2; with atomic density of the composition.

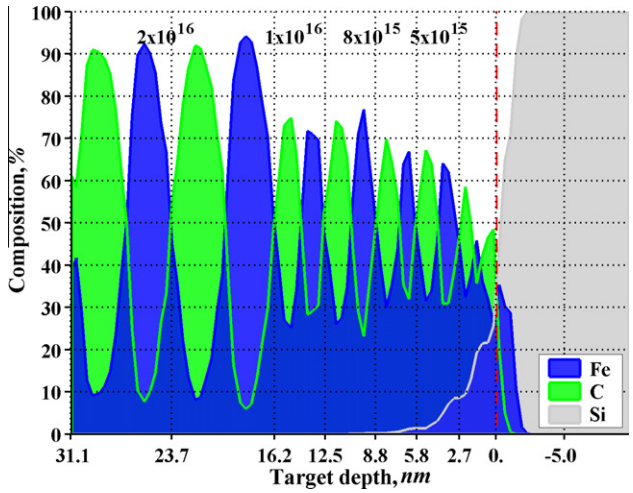

Fig. 5. Four bilayer periods with two bilayers each for fluences of 2×10^{20}, 1×10^{20}, 8×10^{19}, and 5×10^{19} ions/m^2; with atomic density of pure Si.

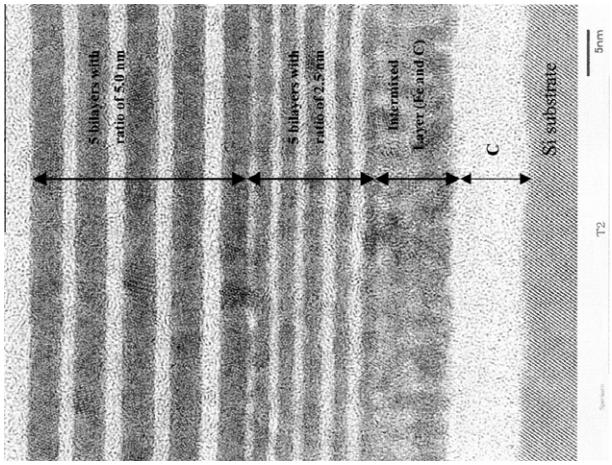

Fig. 6. High-resolution TEM micrograph of Fe/C multilayers with four bilayer periods: 0.75 nm, 1.25 nm, 2.5 nm and 5.0 nm in order from the Si substrate, respectively [23].

times and therefore, each bilayer period consists of five bilayers total.

The thicknesses of the fabricated nanolayers in Fig. 4 differ almost in two times in comparison with nanolayers in Fig. 5, as the atomic density of 50% of iron and 50% of carbon composition, for example, has a value of 9.89×10^{28} m^{-3} while the density of pure Si is 4.98×10^{28} m^{-3}. The results in Fig. 4 are, however, closer to experimental values given in Fig. 6: ~1.1 nm, ~1.8 nm, ~2 nm, and ~4.3 nm.

3.3. Simulations of H ion beams with carbon impurities for ITER-like experiments

To benchmark our models and code in the case of significant influence of the diffusion processes on the implantation and cascade dynamics we considered the recent and very interesting experiments of plasma–material interactions toward the developments of ITER fusion reactor [24]. In these experiments, beams of hydrogen ions containing carbon impurity ions were impinged on pure tungsten samples heated from 653 to 1050 K. Carbon concentration on the surface of tungsten was measured in dependence on the percentage of carbon impurity concentration in the incident ion beams and in dependence on samples temperatures. The incident ion beams consisted of 70% of 333 eV H^+, 10% of 500 eV H^+, 20% of 1000 eV H^+ and from 0.1% to 1% of C ions with 1000 eV energy and various fluences.

Implementing simultaneous particles bombardment and deposition of mixed beams are very important for accurate modeling of the above experiments since the behavior of each particle interactions will influence the processes of the true remaining particles and their interactions. Each component of the ion beams when deposited on the target will change the composition of the sample and therefore, influence the behavior of the subsequent implantation. The deposition of carbon atoms in the form of graphite or in binding with tungsten (WC or W_2C) on the surface of the samples [24] reduces the diffusion of hydrogen in target. For example, the diffusion coefficient of hydrogen isotopes in tungsten has a value of 10^{-10}–10^{-12} m^2/s at the temperature of 650 K [25,26], while this parameter for diffusion of H in randomly oriented carbon at the same temperature is around 1×10^{-20} m^2/s [27]. This large difference will have a significant effect on hydrogen isotopes behavior and retention in candidate plasma facing materials in ITER-like devices. The combined effective diffusion coefficient is assumed in our modeling as the interpolation of the logarithmic values of the individual diffusion coefficient of hydrogen in W and C according to their concentration. We used the values of diffusion coefficients and hydrogen molecular recombination rates that were obtained in the experiments with target temperatures most relevant to our modeled experiments. Also, as hydrogen retention in tungsten and tungsten carbide did not show saturation with the increasing of incident fluence [28] we did not consider the dependence of the hydrogen diffusion coefficient on its concentration in target. Significant chemical erosion of carbon-based materials in the form of CH_4 release due to hydrogen bombardment takes place in the range of temperatures around 500–1000 K [29]. In our modeling when taking into account the dependence on the ions energy and flux, on sample temperature, and on carbon content in the layers, we obtained a chemical erosion yield of 1×10^{-3} atoms/ions. This results in the reduction of carbon concentration at the peak by ~10%.

It was also reported in these experiments that blisters were formed on the target surface at fluence of 3×10^{24} H/m^2 with carbon fraction around 0.8% and at temperatures of 450–650 K [24,30]. We have studied and analyzed in detail and further predicted the conditions of blister formation for different beam-target parameters using the newly developed ITMC-DYN code.

Blisters start to appear with increasing the number density of gas bubbles, and bubbles formation depends on the mobility of implanted gas, the concentration of its atoms in the target, and the rate at which lattice vacancies can be supplied to enhance the stability of a nucleated core. In simulating these experiments, the mobility of hydrogen atoms depends on the modified target composition of W and C. With increasing carbon impurities from 0.11% to 0.84% for the same total fluence of 3×10^{24} m^{-2}, the peak of carbon concentration in target increases from 40% to more than 60% and its location is shifted: 15–20 nm far from the surface in the case of 0.11% and near surface location in the case of 0.84% impurities concentration. This is shown in both the experiments and in our modeling. The range of 333 eV hydrogen ions in tungsten (main component in the mixed beam) is around 5 nm. With little carbon concentration at the surface region, hydrogen was not accumulated in the first case and blisters were not found in the samples. Hydrogen atoms, in this case, recombine and leave the surface or diffuse to the bulk of the sample. In the second case, more than 60% of carbon concentration on the surface results in a significant decrease of the hydrogen diffusion coefficient (in our calculations to 10^{-17} m^2/s) that leads to the high probability of hydrogen retention (Fig. 9). Large numbers of blisters were formed on the surface in this case.

The concentration of hydrogen is then increased with increasing of the total fluence with the same previous conditions as 0.84% of carbon impurities and 653 K temperature of samples. Figs. 7–9 show this dependence for 3×10^{22}, 3×10^{23}, and 3×10^{24} H/m^2 fluences respectively. In these experiments blisters did not appear in the case of low fluence, appeared for the middle fluence, and clearly formed for the high fluence case. Our modeling results showed also the high rate of hydrogen accumulation in the case of 453 K sample temperature (Fig. 10) that explains the high density of large blisters formation found in the sample.

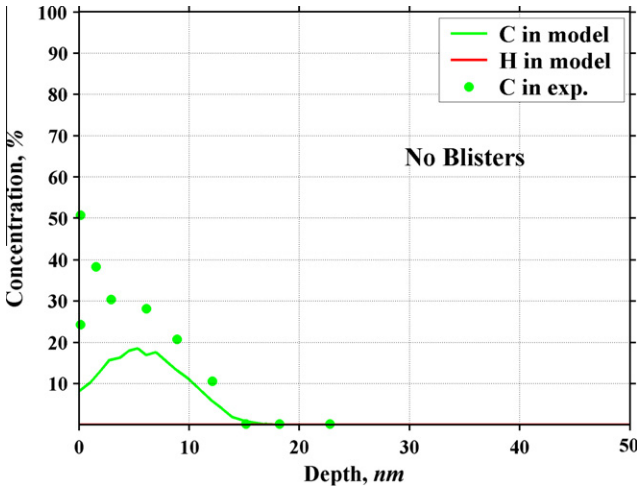

Fig. 7. Concentration of C and H in tungsten sample for fluence of 3×10^{22}/m^2 and sample temperature of 653 K.

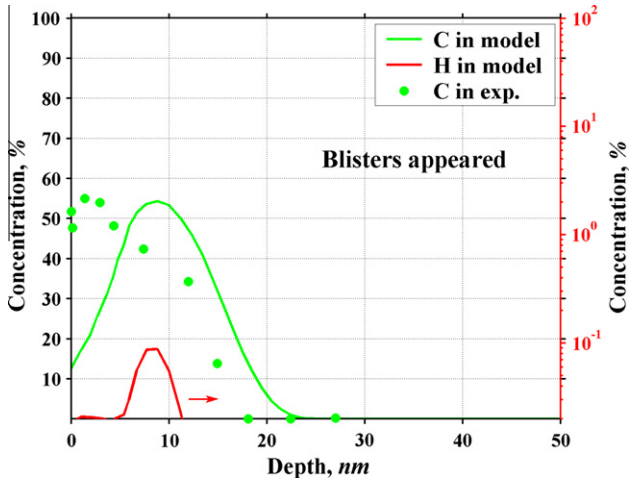

Fig. 8. Concentration of C and H in tungsten sample for fluence of 3×10^{23}/m^2 and sample temperature of 653 K.

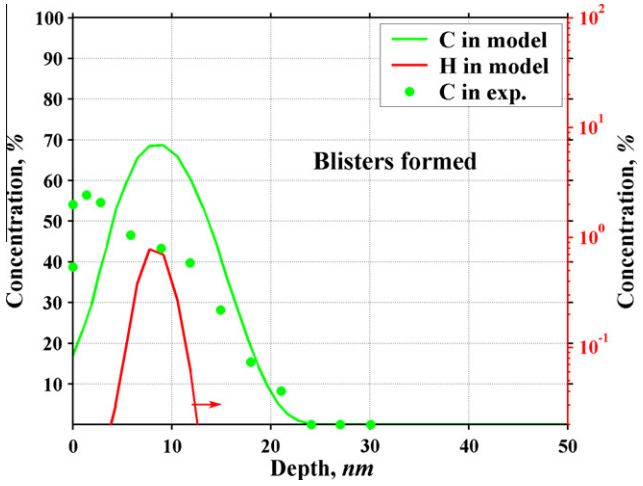

Fig. 9. Concentration of C and H in tungsten sample for fluence of 3×10^{24}/m^2 and sample temperature of 653 K.

Therefore, carbon deposition on the tungsten surface increases hydrogen accumulation because of its low diffusivity in tungsten and carbon composites, especially in sample with 453 K temperature, and it provides conditions for blisters formation in the near surface region. The enhanced ions fluence will provide the additional requirement for blister formation since the damage and vacancies number will increase in tungsten [31].

We implemented two additional and important processes to analyze the difference in the peak location of carbon concentration in the experiments and in our modeling – surface segregation and samples etching by Ar ions.

The process of surface segregation moves carbon atoms from the bulk to the surface layer because of the increase in the chemical potential of carbon in the bulk of W/C compound. Modeling of this phenomenon can shift the peak of the carbon concentration profile to the surface. However if we consider this process self-consistently with ions beam deposition, target atoms sputtering, and atom cascade mixing/redistribution, the effect of surface segregation loses its effectiveness. Carbon atoms moving to the surface will be knocked out by the incident ions beam since the components of beam – hydrogen with 333 eV and carbon with 1 keV energy – have ranges 3–5 nm and the sputtering of C is higher than the sputtering of tungsten: $\sim 1 \times 10^{-2}$ for C by H ions, while H energy is below the threshold for potential sputtering of W. The values of segregation energy were found experimentally for different temperatures and carbon concentrations in tungsten and vary in the range of 2–3 eV [19,20]. We used in our calculations an average value of 2 eV for segregation energy and a reasonable value of 1×10^{-22} m^2/s for calculation of carbon mobility in tungsten for sample temperature of 653 K. The above parameters/results in combination with other considered processes in our modeling predicted sample erosion that is comparable with one found in the experiments of ~100 nm. Increasing of any of these parameters will lead to a significant increase in surface erosion rate.

Surface segregation is a time-dependent process and can take a place at post-irradiation period. Carbon concentration increase on the surface is significant during this time and we also analyzed

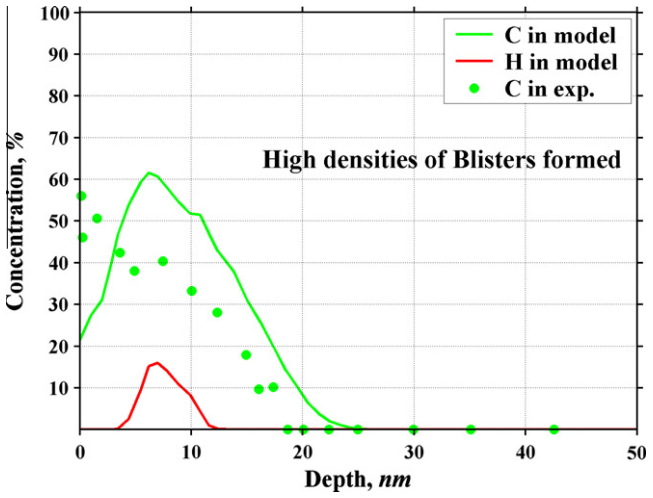

Fig. 10. Concentration of C and H in tungsten sample for fluence of 3×10^{24}/m^2 and sample temperature of 453 K.

the influence of this surface segregation process on the resulting concentration profile.

The concentration profiles given in the experiments were found using the XPS sputter technique. This method provides good depth resolution of sample but has the disadvantages of broadening of the profiles due to the mixing by etching ions beam, and also the preferential sputtering can results in concentrations that differ from the real sample concentration profiles [32]. We modeled the process of etching of the samples by 1.7 keV Ar ions as it was done in these experiments.

Figs. 11 and 12 compare carbon concentrations after the initial deposition of hydrogen and carbon (solid line) and with the subsequent surface segregation and the bombardment of the resulting composite target by Ar ions (dashed line) and with the experimental data. Post-irradiation segregation and etching processes tend to shift the concentration profile towards near the surface and as shown in our modeling it approaches the profile predicted by the experiments.

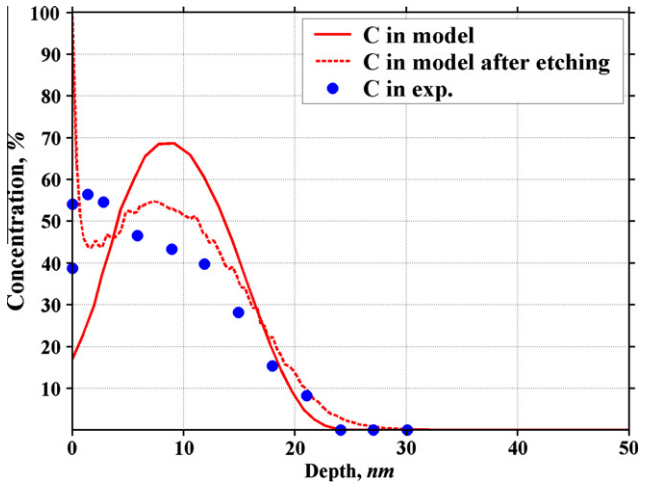

Fig. 11. Concentration of C in tungsten sample after deposition of H with 0.8% C in total fluence $3 \times 10^{24}/m^2$ and sample temperature of 653 K, and with additional process of etching by 1.7 keV Ar ions; dots indicate results from XPS in the experiments [33].

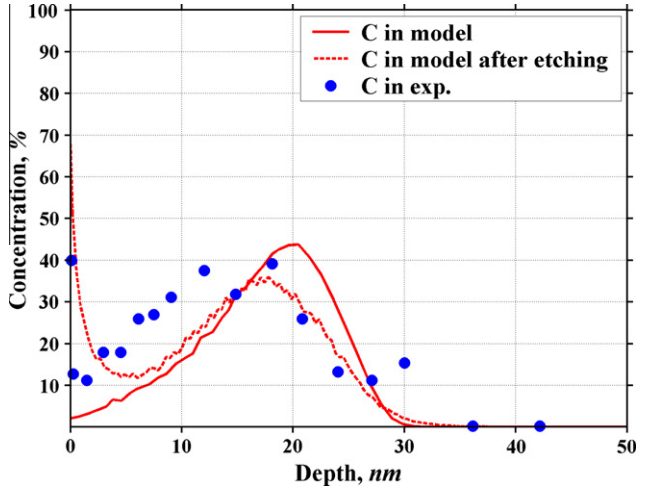

Fig. 12. Concentration of C in tungsten sample after deposition of H with 0.11% C in total fluence $3 \times 10^{24}/m^2$ and sample temperature of 653 K, and with additional process of etching by 1.7 keV Ar ions; dots indicate results from XPS in the experiments [33].

Another important result of our modeling, that can be a good test of the dynamic comprehensive BCA model, is to compare the erosion thicknesses after the initial beam deposition and during the etching process. The predicted surface erosion in these experiments was around 100 nm for all the samples [30]. The calculated thickness of sputtering erosion in modeling was also ~100 nm for 453 K and 653 K sample temperatures for the fluence of 3×10^{24} H/m^2. The correspondence of the etching time with the thickness of the removed material in the modeling is also in good agreement with experiments. Bombarding the target by 1.7 keV Ar ions beam removes 15 nm of samples for 500 s [34].

The distribution and mixing of carbon atoms inside the target in the low temperatures case analyzed above is only due to recoils implantation since carbon diffusivity in tungsten is very low at temperatures below 1000 K. We further studied the dependence of carbon concentration profile on carbon diffusion coefficient and compared the results with the experimental profiles for samples with 1000 K and 1050 K temperatures. The used values of the diffusion coefficients (Fig. 13) are consistent with the values obtained in more recent experiments and in modeling as well [10,35]. In our computer simulation we used the real exposure time of the experiments of 1×10^4 s. This parameter is important for correct modeling of the time-dependent particle diffusion and hydrogen surface recombination processes.

Fig. 13 shows the results of simultaneous ions beam deposition and carbon diffusion in tungsten. The model for surface segregation in these cases with high surface enrichment factor is equivalent to the Fick's law description of diffusion [36]. Segregation of carbon atoms at samples temperatures increases erosion rate but cannot significantly change carbon concentration profile since most carbon atoms moved to the surface are sputtered by the ions beam. Post-ion-irradiation surface segregation and diffusion in the bulk can be the reason of C accumulation on the surface in these experiments. We combined diffusion and the Darken model [36] for the surface segregation to evaluate carbon concentration on the surface at the relatively low temperatures when carbon atoms can still diffuse in tungsten keeping in mind that surface segregation mainly depends on the segregation energy parameter. Fig. 14 demonstrates the influence of these processes during 500 s post-irradiation on the carbon redistribution using diffusion coefficient of 1×10^{-20} m^2/s which corresponds approximately to the temperature of 800 K [35]. Furthermore, during the simulation of

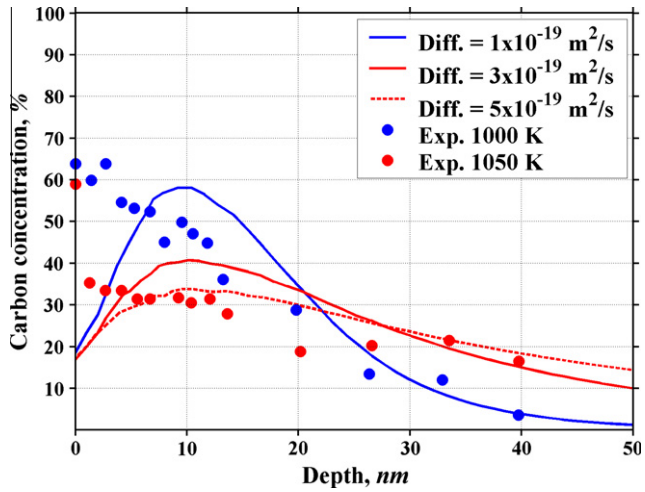

Fig. 13. Concentration of C in tungsten sample for total fluence of $3 \times 10^{24}/m^2$ in modeling with various diffusion coefficients; C profiles in experiments with sample temperatures of 1000 K and 1050 K.

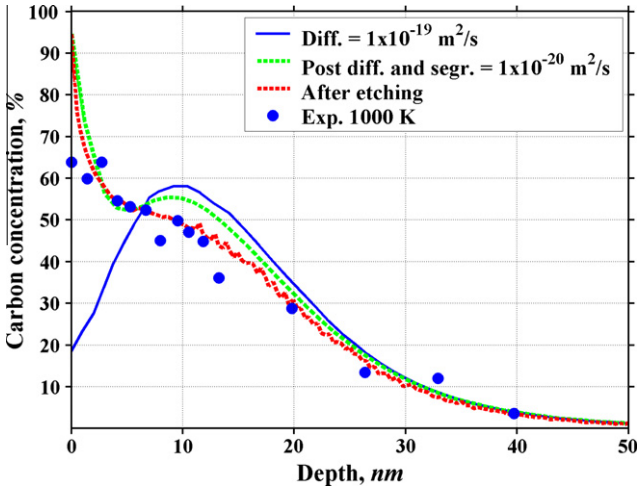

Fig. 14. Concentration of C in tungsten sample for total fluence of $3 \times 10^{24}/m^2$ in modeling with possible post-deposition diffusion and surface segregation; C profiles in experiments with sample temperatures of 1000 K.

the etching process itself using Argon ions, additional correction due to Ar bombardments is made to the final and more accurate carbon concentration profile that better matches the experimental results as shown in Fig. 14.

4. Summary and conclusion

We upgraded our ITMC code to the ITMC-DYN version that now includes the dynamic changing of materials composition, deposition of simultaneous complex ions beams, atom diffusion, chemical erosion, surface segregation and recombination processes, and etching induced redistribution of target atoms. Modeling results and comparison with experiments showed good agreement and therefore, the advantage and potential use of computer simulation to predict and optimize the complex materials behavior in relevant reactor environment.

We studied the dependence of blisters formation in tungsten material on incident ion fluences, impurities content, and samples temperatures. The newly developed models successfully predicted the conditions for blister formation as shown in recent experiments. Parameters such as, the diffusion coefficient of hydrogen in carbon-rich zones can significantly influence the accumulation and the resulting profiles in candidate plasma facing materials such as tungsten. The diffusion parameters obtained from the experiments can vary by several orders of magnitude depending on the experimental conditions and on carbon structure.

Self-consistent implementation of all processes involved in modeling material evolution during ions beam bombardment is quite important in understanding surface erosion, mixed materials evolution, and hydrogen isotope behavior and retention in materials. Low level of impurity contents in plasma, can significantly affect erosion lifetime, largely increase hydrogen isotope retention, and enhance bubble/blister formation in candidate plasma facing materials in reactor environments.

Acknowledgements

Major part of this work is supported by the College of Engineering, Purdue University, and the US Department of Energy, Office of Fusion Energy Sciences.

References

[1] J.P. Biersack, L.G. Haggmark, Nucl. Instrum. Method 174 (1980) 257.
[2] J.F. Ziegler, J.P. Biersack, U. Littmark, The Stopping and Range of Ions in Solids, Pergamon Press, New York, 1985.
[3] W. Möller, W. Eckstein, J.P. Biersack, Comput. Phys. Commun. 51 (1988) 355.
[4] A. Hassanein, Fusion Technol. 8 (1985) 1735.
[5] A. Hassanein, D.L. Smith, Nucl. Instrum. Method B 13 (1986) 225.
[6] A. Hassanein, I. Konkashbaev, J. Nucl. Mater. 273 (1999) 326.
[7] T.A. Mehlhorn, J. Appl. Phys. 52 (N11) (1981) 6522.
[8] C. Varelas, J. Biersack, Nucl. Instrum. Method 79 (1970) 213.
[9] V.B. Berestetskii, E.M. Lifshits, L. Pitaevskii, Quantum Electrodynamics, Pergamon Press, Oxford, New York, 1982.
[10] K. Schmid, J. Roth, J. Nucl. Mater. 302 (2002) 96.
[11] K.L. Wilson, Nucl. Fusion 1 (Special Issue) (1984) (Chapter 3).
[12] M.A. Pick, K. Sonnenberg, J. Nucl. Mater. 131 (1985) 208.
[13] M.I. Baskes, J. Nucl. Mater. 92 (1980) 318.
[14] A. Hassanein, J. Nucl. Mater. 302 (2002) 41.
[15] R.A. Causey, T.J. Venhaus, Phys. Scr. T94 (2001) 9.
[16] J. Roth et al., Nucl. Fusion 44 (2004) L21–L25.
[17] A. Hassanein, V. Morozov, ANL Report, ANL-ET/02-04 (2002).
[18] J. du Plessis, G.N. van Wyk, J. Phys. Chem. Solids 50 (1989) 237.
[19] S.D. Foulias, K.J. Rawlings, B.J. Hopkins, J. Phys. C: Solid State Phys. 14 (1981) 543.
[20] N.D. Potekhina, N.R. Gall', E.V. Rut'kov, A.Ya. Tontegode, Phys. Solid State 45 (N4) (2003) 782.
[21] W. Eckstein, Springer-Verlag, Berlin, Heidelberg, 1991.
[22] A.C. Damask, G.J. Dienes, Point of Defects in Metals, Science, New York, 1963.
[23] Sung-Yong Chun, J. Ceram. Proc. Res. 4 (2003) 115.
[24] Y. Ueda, M. Fukumoto, I. Sawamura, D. Sakizono, T. Shimada, M. Nishikawa, Fusion Eng. Des. 81 (2006) 233.
[25] R. Frauenfelder, J. Vac. Sci. Technol. 6 (1969) 388.
[26] A.P. Zakharov, V.M. Sharapov, E.I. Evko, Fiz.-Khim. Mekh. Mater. 9 (2) (1973) 29–33 (in Russian).
[27] M. Saeki, J. Nucl. Mater. 131 (1985) 32.
[28] K. Sugiyama, K. Krieger, C.P. Lungu, J. Roth, J. Nucl. Mater. 390–391 (2009) 659.
[29] J. Roth, Nuclear Fusion Research, Springer, Berlin, 2004. p. 203.
[30] T. Shimada, T. Funabiki, R. Kawakami, Y. Ueda, M. Nishikawa, J. Nucl. Mater. 329–333 (2004) 747.
[31] V.Kh. Alimov, J. Roth, Phys. Scr. T128 (2007) 6.
[32] K. Schmid, A. Wiltner, Ch. Linsmeier, Nucl. Instrum. Method B 219–220 (2004) 947.
[33] Y. Ueda, T. Shimada, M. Nishikawa, Nucl. Fusion 44 (2004) 62.
[34] R. Kawakami, T. Shimada, Y. Ueda, M. Nishikawa, Jpn. J. Appl. Phys. 42 (2003) 7529.
[35] K. Schmid, J. Roth, W. Eckstein, J. Nucl. Mater. 290–293 (2001) 148.
[36] J. du Plessis, E. Taglauer, Surf. Sci. 260 (1992) 355.